Model-based iterative reconstruction for 320-detector row CT angiography reduces radiation exposure in infants with complex congenital heart disease

Yuzo Yamasaki ⓘ
Takeshi Kamitani ⓘ
Koji Sagiyama ⓘ
Yuko Matsuura ⓘ
Tomoyuki Hida ⓘ
Hazumu Nagata ⓘ

PURPOSE
We investigated the impact of model-based iterative reconstruction (MBIR) on 320-detector row computed tomography angiography (CTA) in infants with complex congenital heart disease (CHD).

METHODS
Seventy infants with complex CHD who underwent 320-detector row CTA (40 boys and 30 girls; age range, 0–22 months; median age, 60 days) were retrospectively evaluated. First, the images were reconstructed by filtered back projection (FBP), hybrid iterative reconstruction (HIR), or MBIR in 20 cases, and variables were compared among the three iterative reconstruction methods (IR test). Second, the variables were compared between 25 cases scanned using HIR and 25 cases scanned using MBIR, with a 20 standard deviation noise level for both. Attenuation values and contrast-to-noise ratios (CNRs) of the great vessels and heart chambers were calculated. Total dose-length products were recorded for all patients (radiation dose: RD test).

RESULTS
In the IR test, the mean CNR values were 4.8±1.3 for FBP, 6.9±1.4 for HIR, and 8.2±1.7 for MBIR (p < 0.0001). The best subjective image qualities in the great vessels and heart chambers were obtained with MBIR. In RD testing, no significant differences between HIR and MBIR in image quality (CNR: HIR, 8.4±2.4; MBIR, 8.3±2.4) were observed. The effective dose was significantly lower for MBIR than for HIR (0.7±0.2 vs. 1.1±0.3 mSv; p < 0.001).

CONCLUSION
The MBIR algorithm significantly improved image quality and decreased radiation exposure in 320-row CTA of infants with complex CHD, providing an alternative to FBP or HIR that is both safer and produces better results.

The prevalence of congenital heart disease (CHD) is gradually increasing and is currently the leading cause of infantile mortality. CHD is documented in approximately 9 per 1000 live births (1, 2). Multidetector computed tomography (CT) has markedly advanced and is widely used for the assessment of infants with complex CHD (3). With this increased use, however, radiation exposure has become a major concern in the treatment of pediatric CHD patients undergoing CT angiography (CTA) (4). Prospective electrocardiogram (ECG)-triggering and a 16 cm z-coverage volume scanning have been shown to be efficient techniques for radiation dose reduction and for obtaining good-quality CTA images in infants who cannot hold their breath (5). Additionally, low-tube voltage scans are also effective in coronary CTA as they lower radiation dose and increase vascular enhancement by moving the x-ray photon energy closer to the k-absorption edge of iodine (6–9). However, low tube voltage scans also increase image noise and decrease image quality.

Recently, a new model-based iterative reconstruction (MBIR) algorithm has been proposed. MBIR can be used for two clinical strategies: 1) improving image quality with the same dose of radiation exposure, and 2) reducing radiation exposure while maintaining image quality. It has been reported that MBIR ameliorates the image quality in pediatric CT (10, 11). In this study, we aimed to demonstrate the utility and applicability of MBIR in infants with complex CHD.

Iterative reconstruction (IR) algorithms reduce image noise; the MBIR technique uses both forward and backward projection according to a statistical metric. Images are creat-

ed using the projection data in backward projection steps; conversely, the projection data are created using the image data in forward projection steps. These forward and backward projections are repeated until they do not change significantly in subsequent iterations or until the maximum number of iterations is reached (12). Hybrid IR (HIR) algorithms mostly use only one backward projection step, whereas MBIR techniques are based on both forward and backward projection steps. Thus, HIR can achieve image reconstruction more rapidly than MBIR; however, the noise reduction is weaker than that with MBIR. One of the concerns with the MBIR algorithm, as compared with FBP and HIR, is that it takes a lot of time to produce the final images, but new computing hardware and algorithmic optimization has enabled faster processing, thus increasing its applicability in clinical practice. Consequently, MBIR is gradually gaining acceptance and becoming more common worldwide.

The purpose of our study was to investigate 1) the impact of MBIR on prospectively ECG-triggered 320-detector row CTA with low-tube voltage in infants with complex CHD, by comparing MBIR images with HIR and filtered back projection (FBP) images, and 2) the radiation exposure reduction of MBIR compared to that of HIR for the same level image quality scan.

Methods

This study was approved by the appropriate institutional review board (protocol number: 29-289) and written informed consent was waived because of the retrospective design. A total of 70 consecutive infant cases having complex CHD (34 boys; age range, 0–22 months) who underwent a 320-detector row CTA with prospectively ECG-gated volume scan, while breathing

freely for cardiovascular evaluation, from January 2017 to January 2018 were enrolled in the study. We defined CHD with 2 or more different cardiovascular anomalies as complex CHD (11). All cardiovascular defects were diagnosed with conventional invasive cardiac angiography and/or surgical findings. We performed 2 types of analysis (described below) to evaluate the capabilities of MBIR.

Effect of iterative reconstruction on image quality using the same raw data set (IR test)

The data from 20 consecutive patients (12 boys and 8 girls; age range, 0–15 months) were reconstructed using FBP, HIR (adaptive iterative dose reduction 3D, Canon Medical Systems), and MBIR (the forward projected model-based iterative reconstruction solution, Canon Medical Systems), and the image qualities were compared to verify the effect of iterative reconstruction among the three image data sets.

Radiation dose comparison between two image series using different iterative reconstructions (RD test)

We included 25 consecutive patients (12 boys and 13 girls; age range, 0–21 months) who underwent scanning using HIR with a 20 standard deviation (SD) noise level (thickness, 0.5 mm) (HIR group), and another 25 consecutive patients (16 boys and 9 girls; age range, 0–22 months) who underwent scanning using MBIR with the same noise level settings (MBIR group). We evaluated image quality and radiation dose to verify the effect of MBIR on radiation exposure.

320-row CTA protocol

All patients underwent CTA with a second-generation 320-detector row CT (Aquilion ONE ViSION edition, Canon Medical Systems), which has a z-axis coverage of 160 mm and rotates in 0.275 s. Patients underwent volume scanning CTA using a prospective ECG-gating while breathing freely. Tube voltage was 80 kVp in every case. The 45% phase of the R–R interval was used for data acquisition. Intravenous thiamylal was used for sedation under cardiorespiratory monitoring. The contrast agent (Iopamiron 300 mg I/mL, Bayer) was administered into a peripheral vein using a dual injector at a rate of 0.033 mL/kg/s for 60 s, followed by a saline chaser at the same rate (0.0033 mL/kg/s) for 20 s. The data was acquired at 80 s. The scan range was changed from 10 cm to 16 cm, based on patient body size and area to be assessed, with the whole chest being scanned. However, the scan range was expanded to the infrahepatic area if inferior vena cava drainage abnormality or heterotaxy was suspected. The system we used allows setting the noise level for automatic tube current modulation under provided image reconstruction mode. The automatic exposure control coordinated the tube current to set the 20 SD noise level in the 0.5 mm thickness with the use of HIR in the HIR group. The noise level of 20 SD in the thickness of 0.5 mm with the use of MBIR was applied in MBIR patients. The scan parameters are shown in Table 1. The estimated effective radiation dose was calculated using the conversion coefficients of the chest, based on patient age and dose-length product (13, 14). Size-specific dose

Table 1. Scan protocols

		RD test	
	IR test	HIR group	MBIR group
Tube voltage (kVp)	80		
Tube current (mAs)	18–48	21–77	18–50
Gantry rotation time (s)	0.275		
Collimation (mm)	0.5×320		
Scan mode	Volume scan		
Z-axis scan range (cm)	10–16		
Predetermined SD level	20		
Slice thickness (mm)	0.5		
Iterative reconstruction	MBIR	HIR	MBIR

IR, iterative reconstruction; RD, radiation dose; HIR, hybrid iterative reconstruction; MBIR, model-based iterative reconstruction; SD, standard deviation.

Table 2. Diagnoses of cardiovascular abnormalities in 20 patients

Parameter	Value
Age (days)	100±110
Sex (male / female)	12 / 8
Body weight (kg)	3.9±1.8
Heart rate (beats per minute)	129±14
Cardiovascular malformations	
Atrial septal defect/patent foramen ovale	8 (16)
Ventricular septal defect	7 (14)
Patent ductus arteriosus	7 (14)
Coarctation of the aorta/hypoplastic aortic arch	4 (8)
Right aortic arch	4 (8)
Pulmonary atresia	4 (8)
Atrioventricular septal defect	3 (6)
Persistent left superior vena cava	3 (6)
Tetralogy of Fallot	2 (4)
Truncus arteriosus communis	2 (4)
Congenitally corrected TGA	1 (2)
Anomalous origin of pulmonary artery	1 (2)
Pulmonary vein stenosis	1 (2)
Double outlet right ventricle	1 (2)
Aortic valve prolapse	1 (2)
Cor triatriatum	1 (2)
Coronary anomalies	1 (2)
Total	49

Continuous variable values are represented as mean±SD. Discrete variable values are represented as n (% of total). TGA, transposition of the great arteries.

estimates (SSDEs) were calculated by multiplying the CT dose index and conversion factor (mGy). Transverse CT images were used to measure anterior-posterior and lateral diameters at the level of the aortic valve (11), and the conversion factors were selected in accordance with the guidelines of the AAPM task group 204 (15).

CT image reconstruction

HIR has 4 levels of noise reduction (strong, standard, mild, and weak), while MBIR has 3 levels (cardiac strong, cardiac standard, and cardiac mild) (10). The standard mode was used in HIR images, and the cardiac standard mode was used in MBIR images. CT data were reconstructed with a 0.5 mm slice interval and 0.5 mm slice thickness. We applied the FC04 kernel for HIR.

Quantitative image quality analysis

All measurements, including the mean CT attenuation of the ascending aorta, the descending aorta, the superior vena cava, the inferior vena cava, the pulmonary trunk, the pulmonary veins, the right atrium, the right ventricle, the left atrium, and the left ventricle were conducted in transverse images by a radiologist who had 8 years of cardiac CT experience. An ellipsoid region of interest (ROI) was set in each structure of interest. The size of each ROI was chosen to be as large as possible and not to approach the edges of structures. CT contrast was defined as the difference between the mean CT attenuation value of the cavity or vessel lumen, and the mean CT attenuation value of the pectoral muscle. Image noise was defined as the SD of the CT attenuation value in a single ROI of the same structure. Lastly, the contrast-to-noise ratio (CNR) was calculated as the ratio of CT contrast and square root of $(SD1^2 + SD2^2)$, where SD1 is the SD of the cavity or vessel lumen and SD2 is the SD of the pectoral muscle. The measurements among the three different reconstructions were compared in the MBIR test, and between the HIR group and MBIR group in the RD test.

Qualitative image quality analysis

Overall image quality was assessed quantitatively by two board-certified radiologists who had over 10 years of cardiac radiology experience. Both radiologists were blinded to the reconstructions used. The evaluations used the following 5-point rubric (16): 5, excellent, all anatomies are clearly observed; 4, good, all structures are interpretable; 3, moderate, the anatomical relationships can be recognized with relative confidence; 2, fair, some anatomical structures are incompletely demonstrated; 1, poor, no relevant information.

In case of disagreement in assessment, a consensus was reached between the observers. Arrangement of window width and level was permitted.

Radiation dose evaluation

The estimated effective dose and SSDEs were evaluated. The effective dose was defined as the result of the dose-length product multiplied by the conversion factor (17, 18). The 16 cm CT dose index phantom was applied. Different conversion coefficients were applied in accordance with the patient age: 0.039 mSv/[mGy.cm] for patients under 4 months; 0.026 mSv/[mGy.cm] for patients 4 months to 1 year old; 0.018 mSv/[mGy.cm] for patients 1 year to 2 years old, following previous reports (4, 13, 16). SSDEs were calculated using axial CT images. Lateral and anterior-posterior diameters of the chest were measured. In each case, the conversion factors were applied in accordance with the sum of these diameters using the AAPM task group 204 report (15).

Statistical analysis

Statistical analyses were conducted using JMP statistical software (version 14.2.0; SAS Institute). Numerical data are expressed as mean±SD. The Shapiro-Wilk test was used to assess normality distribution. When the variables were normally distributed, a one-way analysis of variance (ANOVA) was used to compare mean values among the three reconstruction techniques. When the variables were non-normally distributed, the Kruskal-Wallis test was used to compare median values among the three reconstruction techniques. If significant differences were observed among the groups,

Table 3. Comparison of contrast-to-noise ratios in the IR test

	FBP	HIR	MBIR	*p*
Ascending aorta	5.1±1.4	7.6±1.6	9.3±2.0	<0.0001*
Descending aorta	4.9±1.5	7.2±1.8	9.1±3.1	<0.0001*
Superior vena cava	4.2±1.1	5.9±1.4	6.7±1.6	<0.0001*
Inferior vena cava	4.1±1.3	5.7±1.6	7.0±2.1	<0.0001*
Pulmonary artery	4.9±1.3	7.5±1.9	9.3±2.5	<0.0001*
Pulmonary vein	4.6±1.5	6.7±1.7	8.3±2.2	<0.0001*
Right atrium	4.8±1.2	6.9±1.4	7.9±1.7	<0.0001*
Right ventricle	5.2±1.5	7.6±1.9	9.0±2.4	<0.0001*
Left atrium	4.9±1.7	7.4±1.9	8.9±2.4	<0.0001*
Left ventricle	5.0±1.5	7.5±2.1	8.8±2.7	<0.0001*
All locations	4.8±1.3	6.9±1.4	8.2±1.7	<0.0001*

Data are represented as mean±SD.
FBP, filtered back-projection; HIR, hybrid iterative reconstruction; MBIR, model-based iterative reconstruction.
*Significant differences for all comparison combinations among the three methods.

Table 4. Comparison of the quality of the images in the IR test

	FBP	HIR	MBIR	*p*
Ascending aorta	3.3±0.5	3.7±0.6	4.4±0.6	<0.0001*
Descending aorta	2.9±0.4	3.6±0.6	4.3±0.7	<0.0001*
Superior vena cava	3.0±0.5	3.6±0.7	4.2±0.8	0.0008*
Inferior vena cava	2.9±0.6	3.6±0.6	4.2±0.7	0.0004*
Pulmonary artery	3.3±0.6	3.7±0.7	4.5±0.5	<0.0001*
Pulmonary vein	3.0±0.6	3.7±0.6	4.4±0.7	0.0002*
Right atrium	3.2±0.6	3.6±0.6	4.3±0.5	0.0002*
Right ventricle	3.2±0.5	3.7±0.6	4.3±0.6	0.0001*
Left atrium	3.1±0.5	3.7±0.6	4.2±0.6	<0.0001*
Left ventricle	3.1±0.5	3.7±0.6	4.2±0.7	0.0003*
All locations	3.1±0.4	3.6±0.5	4.3±0.5	<0.0001*

Data are represented as mean±SD.
FBP, filtered back-projection; HIR, hybrid iterative reconstruction; MBIR, model-based iterative reconstruction.
*Significant differences for all comparison combinations among the three methods.

pairwise comparisons were conducted with the Steel-Dwass test. A Bonferroni correction was applied for multiple comparisons. The Mann-Whitney U test was used to compare two groups. We analyzed the ordinal data using nonparametric tests (the Mann-Whitney U test for two variables and the Kruskal-Wallis and the Steel-Dwass tests for multiple comparisons). Two-sided *P* values of less than 0.05 were considered statistically significant. Study sample sizes required to detect a significant difference in CNR among FBP, HIR, and MBIR, and a radiation exposure of 1.0 mGy between HIR and MBIR were calculated with a power of 0.8 and an error of 0.05. The required sample sizes were 9 and 34, respectively.

Results

Effect of iterative reconstruction on image quality using a single raw data set (IR test)

Diagnoses of cardiovascular anomalies in 20 cases are shown in Table 2.

Quantitative image quality

The mean CT image noise of all structures for FBP, HIR, and MBIR images was 37.7±9.5, 27.5±5.0, and 23.5±4.4 HU, respectively. Statistically significant differences were observed for all comparison assortments among the three reconstructions (*p* < 0.001) (Supplementary Table S1). No significant differences were observed in CT attenuation values among the three recon-

structions at any structures (Supplementary Table S2). The CNR of MBIR was significantly higher than those of FBP and HIR at every evaluated structure (*p* < 0.01; Table 3).

Qualitative image quality

Results are shown in Table 4 and Fig. 1. The visual quantitative scores were significantly better for MBIR than the other reconstructions (*p* < 0.01), and the scores for the HIR images were significantly better than those for FBP (*p* < 0.01).

Radiation dose comparison between two image series using distinct iterative reconstructions (RD test)

No significant differences were observed in the clinical parameters (age, sex, body weight, and heart rate) between the HIR and MBIR groups. Diagnoses of cardiovascular deformities in the HIR group and MBIR group are shown in Table 5.

Quantitative image quality

Image noise and attenuation values of HIR and MBIR groups are shown in Supplementary Tables S3 and S4. The mean CNR values of the HIR and the MBIR group images were 8.4±2.4 and 8.3±2.4, respectively (Table 6). No significant difference was observed between the two groups (*p* = 0.96).

Quantitative image quality

No significant differences were observed in the visual scores between the two groups (Table 7).

Radiation dose

The mean dose-length product was 37.3±17.6 mGy·cm in the HIR group and 22.5±11.5 mGy·cm in the MBIR group. The mean estimated effective dose was 1.1±0.3 mSv in the HIR group and 0.7±0.2 mSv in the MBIR group (*p* < 0.001) (Fig. 2). The mean SSDE was 3.9±1.5 mGy in the HIR group and 2.8±1.5 mGy in the MBIR group (*p* < 0.05) (Fig. 2). Radiation doses were significantly smaller in the MBIR group than in the HIR group. Representative cases are shown in Figs. 3 and 4.

Discussion

In this study, we compared quantitative and qualitative image quality among three reconstruction techniques. The major findings of our study are: 1) the image quality of MBIR was significantly better than that of FBP and HIR; and 2) MBIR reduced radia-

Table 5. Diagnoses of cardiovascular abnormalities in HIR and MBIR groups

	HIR (n=25)	MBIR (n=25)
Age (days)	146±187	133±160
Sex (male/female)	11/14	15/10
Body weight (kg)	4.3±2.7	4.2±2.1
Heart rate (beats per minute)	133±15	130±15
Cardiovascular malformations		
Atrial septal defect/patent foramen ovale	10	10
Ventricular septal defect	9	7
Patent ductus arteriosus	8	8
Pulmonary atresia/stenosis	7	3
Coarctation of the aorta / hypoplastic aortic arch	4	5
Right aortic arch	6	3
Atrioventricular septal defect	3	5
Total anomalous pulmonary venous return	2	4
Pulmonary vein stenosis	4	2
Persistent left superior vena cava	4	1
Tetralogy of Fallot	2	2
Single ventricle	2	1
Anomalous origin of pulmonary artery	2	1
Congenitally corrected TGA	2	1
Mitral stenosis/atresia	2	1
Partially anomalous pulmonary venous return	1	1
Double outlet right ventricle	1	1
Coronary anomalies	1	1
Aortic valve prolapse	0	2
Cor triatriatum	0	1
Interrupted aortic arch	1	0
Truncus arteriosus communis	1	0
Total	72	60

HIR, hybrid iterative reconstruction; MBIR, model-based iterative reconstruction; TGA, transposition of the great arteries.

Table 6. Comparison of contrast-to-noise ratios in the RD test

	HIR	MBIR	*p*
Ascending aorta	8.8±2.3	9.1±2.6	0.70
Descending aorta	8.7±3.0	8.9±3.4	0.82
Superior vena cava	8.0±2.3	7.6±2.3	0.27
Inferior vena cava	7.2±2.6	7.6±2.6	0.64
Pulmonary artery	8.5±2.6	9.1±2.9	0.44
Pulmonary vein	8.8±3.1	8.5±3.2	0.68
Right atrium	8.1±2.6	8.1±2.5	0.78
Right ventricle	9.2±3.1	8.9±2.9	0.62
Left atrium	8.6±2.8	8.5±2.9	0.85
Left ventricle	9.0±2.9	8.5±2.7	0.59
All locations	8.4±2.4	8.3±2.4	0.96

Data are represented as mean±SD.
RD, radiation dose; HIR, hybrid iterative reconstruction; MBIR, model-based iterative reconstruction.

tion exposure while maintaining the image quality when compared to HIR.

Conventional invasive cardiac angiography has been a recognized reference standard in the assessment of complex CHD, but cardiac catheterization of infants, especially those with complex CHD, can be difficult due to the small body size of the patients and their inability to cooperate. In addition, conventional cardiac angiography is an invasive method and has an approximately 0.1%–0.3% intraoperative mortality rate (19, 20), as well as the potential for a high radiation dose (21). The mean effective dose of pediatric cardiac catheterization to diagnose CHD has been reported to be approximately 13 mSv (18, 22), while the results of our study show that the mean radiation dose using MBIR was just 0.7 mSv. Thus, the MBIR algorithm can be applied with reasonable radiation doses. In accordance with the "ALARA" principle, radiologists must minimize radiation exposure as much as is reasonably achievable.

CT is effective in demonstrating extracardiac findings, such as pulmonary artery anatomy and significant aortopulmonary collateral vessels, and is also useful for accurate depiction of thoracic aorta and pulmonary veins and their structural relationships (3, 4). CT provides important complimentary information to transthoracic echocardiography.

The advantage of a wide array detector is greater z-axis coverage, as it enables a 16 cm coverage volume scan in a single rotation. This reduced the helical scan time and resulted in the reduction of radiation exposure. Moreover, short scan times help to obtain more static images, especially for infants too young to stop their motion intentionally. In addition, the use of MBIR further improved the image quality as compared to FBP and HIR. These findings are in line with those of previous studies that prove the utility of wide array detector CT or MBIR (3, 5, 10, 11, 13). In this study, we also demonstrated the clinical utility of the combination of wide array detector CT and MBIR in infants with CHD.

As previously mentioned, our results show that MBIR reduces radiation exposure while maintaining image quality during the evaluation of complex CHD using 320-row CTA. This is of practical importance, as ECG-triggered free-breathing 320-row CTA
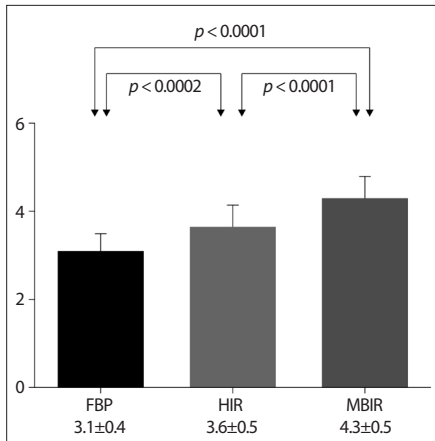
Figure 1. Comparison of qualitative image qualities. Bar plots show the mean and the standard error of the mean for filtered back-projection (FBP), hybrid iterative reconstruction (HIR), and model-based iterative reconstruction (MBIR). Image quality was significantly different among the three reconstruction methods.

Table 7. Comparison of the quality of the images in the RD test

	HIR	MBIR	p
Ascending aorta	4.5±0.5	4.5±0.6	0.99
Descending aorta	4.3±0.7	4.3±0.8	0.95
Superior vena cava	4.2±0.6	4.2±0.8	0.93
Inferior vena cava	4.1±0.6	4.1±0.7	0.98
Pulmonary artery	4.4±0.7	4.6±0.5	0.52
Pulmonary vein	4.2±0.7	4.4±0.7	0.37
Right atrium	4.4±0.5	4.3±0.5	0.56
Right ventricle	4.4±0.6	4.4±0.6	0.88
Left atrium	4.4±0.6	4.3±0.7	0.74
Left ventricle	4.4±0.6	4.2±0.7	0.23
All locations	4.3±0.5	4.3±0.6	0.88

Data are represented as mean±SD.
RD, radiation dose; HIR, hybrid iterative reconstruction; MBIR, model-based iterative reconstruction.
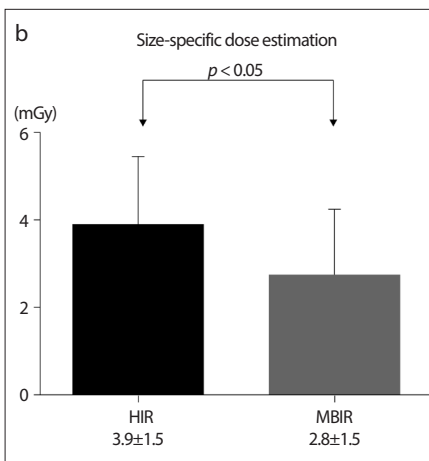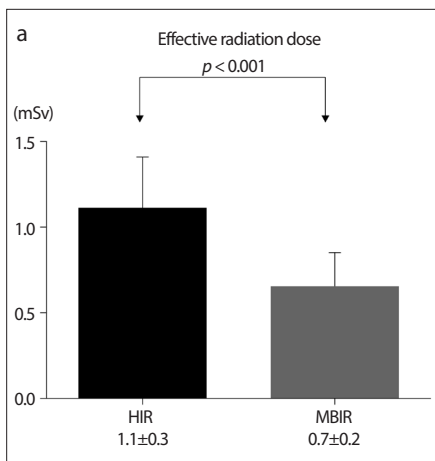

Figure 2. a, b. Comparison of radiation exposures. Bar plots show the mean and the standard error of the mean, HIR, and MBIR. The mean effective dose was significantly lower for MBIR than for HIR in both effective radiation dose (a) and size-specific dose estimation (b).
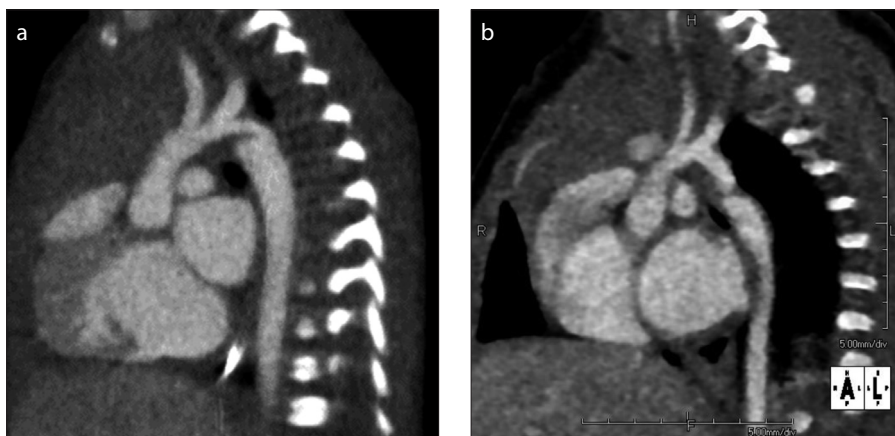

Figure 3. a, b. Images of infants with coarctation of the aorta. Oblique sagittal images of a 10-day-old boy in the HIR group (a) and a 2-month-old boy in the MBIR group (b). Contrast-to-noise ratio (CNR) was slightly higher in HIR than MBIR (HIR 16.0 vs. MBIR 12.5); however, radiation dose in MBIR was smaller than that in HIR (effective radiation dose : HIR 0.92 mSv vs. MBIR 0.55 mSv; size-specific dose estimate, HIR 2.45 mGy vs. MBIR 1.61 mGy).

with MBIR contributes to the reduction of radiation exposure without hampering the diagnostic image qualities in infants who would otherwise undergo diagnostic and repeated follow-up CT scans. While the noise reduction technique is essential for good image quality, it is sometimes associated with a loss of spatial resolution. However, MBIR has been shown to reduce image noise while maintaining the spatial resolution (10). This is crucial for the evaluation of small structures in infants. Taken together, our results and those of previous studies suggest that using the MBIR algorithm is a good option for image reconstruction in neonatal patients.

Cardiac magnetic resonance imaging (MRI) is an established diagnostic tool for the evaluation of cardiac anatomy and function. It might be an alternative to cardiac catheterization as well, which is not associated with any radiation exposure at all. However, cardiac MRI in neonates requires relatively long scan times and general anesthesia with intubation. In addition, high heart rates in neonates pose technical challenges. MRI with anesthesia is generally safe; however, there is a high risk of adverse anesthetic events with MRI in hospitalized and neonatal patients. The relative risk of an adverse event during cardiac MRI if performed with anesthesia is 3.9 (23–25). Furthermore, repeated or prolonged use of general anesthetics or sedatives during early childhood could be associated with negative effects on the developing brain (26–29). The short imaging time of CT could therefore be clinically useful.
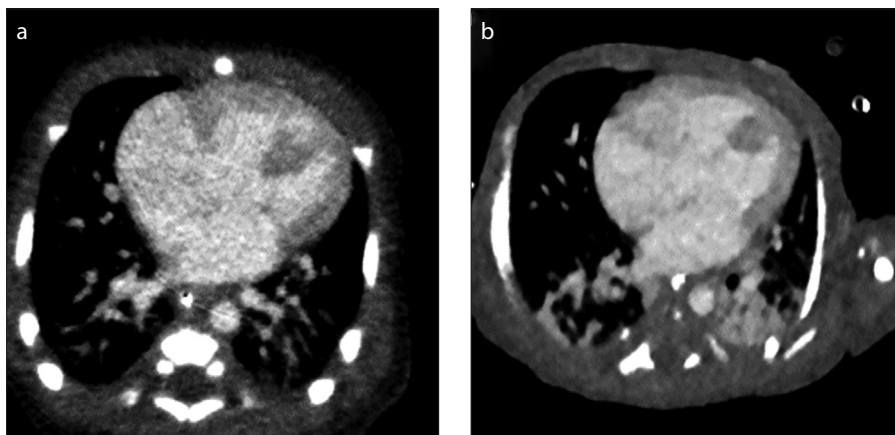
Figure 4. a, b. Images of infants with complete atrioventricular septal defect. Axial images of a 10-day-old boy in the HIR group (**a**) and an 11-day-old boy in the MBIR group (**b**). CNR was higher in MBIR than HIR (HIR 10.4 vs. MBIR 18.1). Moreover, radiation dose was also very small in MBIR compared to that in HIR (effective radiation dose, HIR 0.94 mSv vs. MBIR 0.36 mSv; size-specific dose estimate, HIR 2.72 mGy vs. MBIR 1.25 mGy).

This study has several limitations that should be acknowledged. First, the size of our study population was rather small; further studies with larger cohorts are required in the future. Second, we used a combination of prospectively ECG-gated scans and a low tube voltage. Also, we applied novel iterative reconstruction in order to decrease the radiation dose. However, the radiation dose in the present study was still higher than that reported by previous studies using 320-row CT or dual source CT (4, 13). The wide craniocaudal-directional coverage used in the current study may account for these discrepancies. In addition, the patients with complex CHD also had a high prevalence of extracardiac malformations, such as tracheal anomalies, thymus deficiencies, and isomerism. Thus, assessing these extracardiac abnormalities are essential for the clinical management of complex CHD. Another possibility for these discrepancies is the setting of image noise while scanning. Recently, Shirota et al. (11) reported the utility of a predetermined level of image noise set at an SD of 40. This could reduce over 50% of radiation exposure when compared with the SD 20 setting, although the corresponding image quality obtained must be checked. Finally, because of the retrospective nature of this study, there are limitations of bias inherent to the study design. Additionally, the results cannot be extrapolated to other populations with CHD (e.g., older children or simple CHD).

In conclusion, implementing a novel MBIR algorithm reduced the radiation exposure while maintaining the image quality, in free-breathing and prospectively ECG-triggered 320-row CTA of infants with complex CHD.

Conflict of interest disclosure

The authors declared no conflicts of interest.

References

1. van der Linde D, Konings EE, Slager MA, et al. Birth prevalence of congenital heart disease worldwide: a systematic review and meta-analysis. J Am Coll Cardiol 2011; 58:2241–2247. [Crossref]
2. Xie D, Fang J, Liu Z, et al. Epidemiology and major subtypes of congenital heart defects in Hunan Province, China. Medicine (Baltimore) 2018; 97:e11770. [Crossref]
3. Yamasaki Y, Kawanami S, Kamitani T, et al. Free-breathing 320-row computed tomographic angiography with low-tube voltage and hybrid iterative reconstruction in infants with complex congenital heart disease. Clin Imaging 2018; 50:147–156. [Crossref]
4. Cheng Z, Wang X, Duan Y, et al. Low-dose prospective ECG-triggering dual-source CT angiography in infants and children with complex congenital heart disease: first experience. Eur Radiol 2010; 20:2503–2511. [Crossref]
5. Jadhav SP, Golriz F, Atweh LA, Zhang W, Krishnamurthy R. CT angiography of neonates and infants: comparison of radiation dose and image quality of target mode prospectively ECG-gated 320-MDCT and ungated helical 64-MDCT. AJR Am J Roentgenol 2015; 204:W184–W191. [Crossref]
6. Schueller-Weidekamm C, Schaefer-Prokop CM, Weber M, Herold CJ, Prokop M. CT angiography of pulmonary arteries to detect pulmonary embolism: improvement of vascular enhancement with low kilovoltage settings. Radiology 2006; 241:899–907. [Crossref]
7. Sigal-Cinqualbre AB, Hennequin R, Abada HT, Chen X, Paul JF. Low-kilovoltage multi–detector row chest CT in adults: feasibility and effect on image quality and iodine dose. Radiology 2004; 231:169–174. [Crossref]
8. Nakayama Y, Awai K, Funama Y, et al. Lower tube voltage reduces contrast material and radiation doses on 16-MDCT aortography. AJR Am J Roentgenol 2006; 187:W490–W497. [Crossref]
9. Yuki H, Utsunomiya D, Funama Y, et al. Value of knowledge-based iterative model reconstruction in low-kV 256-slice coronary CT angiography. J Cardiovasc Comput Tomogr 2014; 8:115–123. [Crossref]
10. Nishiyama Y, Tada K, Nishiyama Y, et al. Effect of the forward-projected model-based iterative reconstruction solution algorithm on image quality and radiation dose in pediatric cardiac computed tomography. Pediatr Radiol 2016; 46:1663–1670. [Crossref]
11. Shirota G, Maeda E, Namiki Y, et al. Pediatric 320-row cardiac computed tomography using electrocardiogram-gated model-based full iterative reconstruction. Pediatr Radiol 2017; 47:1463–1470. [Crossref]
12. den Harder AM, Willemink MJ, Budde RP, Schilham AM, Leiner T, de Jong PA Hybrid and model-based iterative reconstruction techniques for pediatric CT. AJR Am J Roentgenol 2015; 204:645–653. [Crossref]
13. Zhang T, Wang W, Luo Z, et al. Initial experience on the application of 320-row CT angiography with low-dose prospective ECG-triggered in children with congenital heart disease. Int J Cardiovasc Imaging 2012; 28:1787–1797. [Crossref]
14. Valentin J. Managing patient dose in multi-detector computed tomography (MDCT). New York: Elsevier, 2007.
15. Boone JM, Strauss KJ, Cody DD, McCollough CH, McNitt-Gray MF, Toth TL. Size-specific dose estimates (SSDE) in pediatric and adult body CT examinations. Report of AAPM Task Group 204. College Park, MD, USA: American Association of Physicists in Medicine; 2011. 26 p. Report No: 204. [Crossref]
16. Ben Saad M, Rohnean A, Sigal-Cinqualbre A, Adler G, Paul JF. Evaluation of image quality and radiation dose of thoracic and coronary dual-source CT in 110 infants with congenital heart disease. Pediatr Radiol 2009; 39:668–676. [Crossref]
17. Stolzmann P, Scheffel H, Schertler T, et al. Radiation dose estimates in dual-source computed tomography coronary angiography. Eur Radiol 2008; 18:592–599. [Crossref]
18. Einstein AJ, Moser KW, Thompson RC, Cerqueira MD, Henzlova MJ. Radiation dose to patients from cardiac diagnostic imaging. Circulation 2007; 116:1290–1305. [Crossref]
19. Vitiello R, McCrindle BW, Nykanen D, Freedom RM, Benson LN. Complications associated with pediatric cardiac catheterization. J Am Coll Cardiol 1998; 32:1433–1440. [Crossref]
20. Mori Y, Takahashi K, Nakanishi T. Complications of cardiac catheterization in adults and children with congenital heart disease in the current era. Heart Vessels 2013; 28:352–359. [Crossref]
21. Bacher K, Bogaert E, Lapere R, De Wolf D, Thierens H. Patient-specific dose and radiation risk estimation in pediatric cardiac catheterization. Circulation 2005; 111:83–89. [Crossref]

22. Karambatsakidou A, Sahlgren B, Hansson B, Lidegran M, Fransson A. Effective dose conversion factors in paediatric interventional cardiology. Br J Radiol 2009; 82:748–755. [Crossref]

23. Girshin M, Shapiro V, Rhee A, Ginsberg S, Inchiosa MA, Jr. Increased risk of general anesthesia for high-risk patients undergoing magnetic resonance imaging. J Comput Assist Tomogr 2009; 33:312–315. [Crossref]

24. Dorfman AL, Odegard KC, Powell AJ, Laussen PC, Geva T. Risk factors for adverse events during cardiovascular magnetic resonance in congenital heart disease. J Cardiovasc Magn Reson 2007; 9:793–798. [Crossref]

25. Slovis TL. Sedation and anesthesia issues in pediatric imaging. Pediatr Radiol 2011; 41 (Suppl 2):514–516. [Crossref]

26. Flick RP, Katusic SK, Colligan RC, et al. Cognitive and behavioral outcomes after early exposure to anesthesia and surgery. Pediatrics 2011; 128:e1053–1061. [Crossref]

27. Wilder RT, Flick RP, Sprung J, et al. Early exposure to anesthesia and learning disabilities in a population-based birth cohort. Anesthesiology 2009; 110:796–804.[Crossref]

28. Ing C, DiMaggio C, Whitehouse A, et al. Long-term differences in language and cognitive function after childhood exposure to anesthesia. Pediatrics 2012; 130:e476–485. [Crossref]

29. DiMaggio C, Sun LS, Kakavouli A, Byrne MW, Li G. A retrospective cohort study of the association of anesthesia and hernia repair surgery with behavioral and developmental disorders in young children. J Neurosurg Anesthesiol 2009; 21:286–291. [Crossref]

Supplementary Table S1. Comparison of image noise in the IR test (n=20)

	FBP	HIR	MBIR	p
Ascending aorta	35.2±12.4	24.9±5.7	20.2±4.1	<0.0001*
Descending aorta	36.4±12.5	26.2±6.6	20.9±5.4	<0.0001*
Superior vena cava	46.8±12.1	37.4±11.7	35.2±14.2	0.0028*
Inferior vena cava	36.0±13.0	27.6±9.4	22.2±8.9	<0.0001*
Pulmonary artery	37.9±11.2	25.7±5.6	21.0±4.6	<0.0001*
Pulmonary vein	40.7±13.6	29.6±9.8	24.1±8.1	0.0002*
Right atrium	36.5±13.5	27.6±9.6	25.3±11.7	<0.0001*
Right ventricle	33.8±8.0	24.9±3.2	21.7±3.7	<0.0001*
Left atrium	36.9±9.3	25.3±3.4	21.1±2.6	<0.0001*
Left ventricle	36.4±8.9	26.2±4.5	23.2±5.1	<0.0001*
All locations	37.7±9.5	27.5±5.0	23.5±4.4	<0.0001*

Data are presented as mean ± standard deviation. IR, iterative reconstruction; FBP, filtered back-projection; HIR, hybrid iterative reconstruction; MBIR, model-based iterative reconstruction. *Significant differences for all comparison combinations among the three methods.

Supplementary Table S2. Comparison of attenuation values in the IR test (n=20)

	FBP	HIR	MBIR	p
Ascending aorta	319.8±56.0	319.7±56.0	321.4±57.8	0.99
Descending aorta	312.0±61.9	311.7±60.7	314.7±64.0	0.98
Superior vena cava	316.1±68.8	317.9±71.1	319.1±72.3	0.97
Inferior vena cava	274.5±92.8	273.9±90.5	270.5±85.9	0.99
Pulmonary artery	316.6±53.9	316.0±54.1	319.2±56.1	0.99
Pulmonary vein	306.6±54.1	305.0±52.9	309.6±57.1	0.93
Right atrium	310.7±66.6	310.6±66.4	309.7±65.2	0.99
Right ventricle	317.7±61.5	317.5±62.0	321.9±62.3	0.92
Left atrium	313.1±64.4	312.8±64.5	312.6±65.3	0.99
Left ventricle	318.1±66.5	317.9±66.7	321.5±65.7	0.94
All locations	310.5±59.1	310.3±59.0	312.0±59.3	0.97

Data are presented as mean ± standard deviation. IR, iterative reconstruction; FBP, filtered back-projection; HIR, hybrid iterative reconstruction; MBIR, model-based iterative reconstruction.

Supplementary Table S3. Comparison of image noise in the RD test

	HIR (n=25)	MBIR (n=25)	p
Ascending aorta	21.8±4.3	19.3±3.8	0.04*
Descending aorta	22.4±5.5	20.8±5.4	0.29
Superior vena cava	25.3±7.7	26.2±6.8	0.53
Inferior vena cava	24.2±5.5	20.1±8.3	0.005*
Pulmonary artery	22.2±4.1	20.3±5.0	0.18
Pulmonary vein	21.7±4.4	21.4±8.0	0.14
Right atrium	24.1±3.0	23.4±11.4	0.10
Right ventricle	20.5±4.0	21.0±3.7	0.70
Left atrium	22.4±3.3	20.9±2.6	0.11
Left ventricle	21.3±3.2	22.3±5.1	0.38
All locations	22.4±2.5	21.6±3.8	0.07

Data are the mean ± standard deviation. RD, radiation dose; HIR, hybrid iterative reconstruction; MBIR, model-based iterative reconstruction. *Significant difference between the two methods.

Supplementary Table S4. Comparison of attenuation values in the RD test			
	HIR (n=25)	MBIR (n=25)	*p*
Ascending aorta	316.5±76.2	309.8±77.7	0.79
Descending aorta	313.4±77.6	306.9±83.8	0.80
Superior vena cava	310.1±69.5	306.0±71.8	0.83
Inferior vena cava	286.6±78.3	271.5±90.5	0.43
Pulmonary artery	306.4±76.6	309.1±78.9	0.92
Pulmonary vein	311.0±78.2	300.3±77.8	0.89
Right atrium	308.5±75.9	302.6±78.6	0.88
Right ventricle	312.6±78.1	312.0±78.7	0.97
Left atrium	312.0±77.8	300.8±80.6	0.61
Left ventricle	315.6±79.6	310.0±79.2	0.79
All locations	308.0±74.5	302.9±74.9	0.83
Data are the mean ± standard deviation. RD, radiation dose; HIR, hybrid iterative reconstruction; MBIR, model-based iterative reconstruction.			